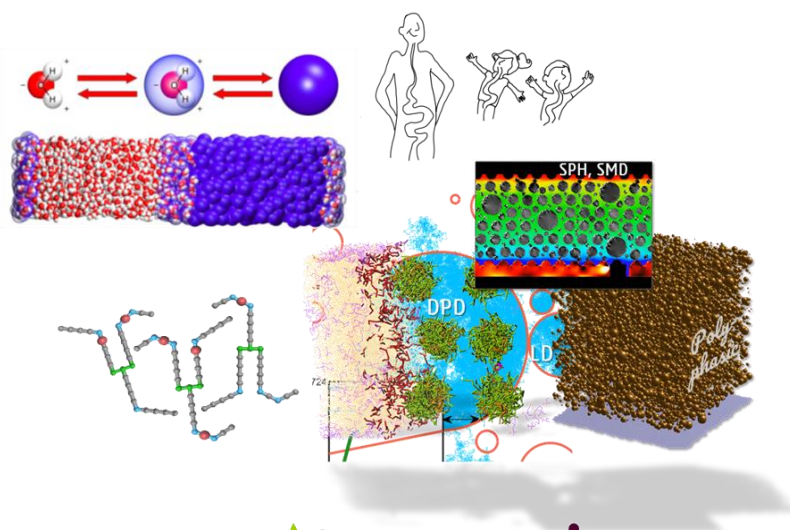


Stage de fin d'année  
Master 1  
Génie des procédés – (Energie et Procédés)

Coarse grain modeling of mass transfer phenomena  
occurring during food deconstruction



# Acknowledgements

First of all, I would like to give my heartfelt thanks to all the people who have ever helped me in this paper.

My sincere and hearty thanks and appreciations go firstly to my supervisor, Mr. Olivier Vitrac. He gave me the opportunity to do an internship in his lab so that I could gain a more in-depth understanding of the differences between scientific work and engineering work. He is a man who is very serious about research and seeks truth and facts, and that has deeply influenced me. He is also a humorous and curious person, and this optimistic and positive attitude towards life also makes me look forward to a life of research. It was a great privilege and pleasure to study under his guidance and supervision. Furthermore, it is my honor to benefit from his personality and diligence, which I will treasure my whole life. My gratitude to him knows no bounds.

I also would like to thank William Jenkinson, the PH. D student of Olivier, for bringing me forward in experiences, discuss with me patiently and answer many of my questions.

Especially this thesis owes a debt to other students in the lab, Hawraa Ayoub, Julien Kermorvant, Natacha Daoud and Lucas Biant, who are kindness and openness, give me substantial support and urge me to do better in language study and research, and they also created an enjoyable working environment.

Finally, I am really grateful to all those who devote much time to reading this thesis and give me much advice, which will benefit me in my later study.

# Content

<i>Abstract</i> .....	7
<i>1 Introduction</i> .....	8
1.1 The research group MODIC .....	8
1.2 Research objective .....	11
1.3 Document outline .....	11
<i>2 Short review of meshless simulation methods at mesoscale</i> .....	12
2.1 What is the mesoscale .....	12
2.2 Coarse-graining modeling methodology .....	14
2.3 Specific techniques in multiscale modeling .....	15
2.4 Intermediate summary .....	17
<i>3 Goals and approaches</i> .....	18
3.1 Work plan: intermediate and final goals .....	18
3.2 Main goals .....	19
3.3 Approaches followed .....	21
<i>4 Methodology</i> .....	23
4.1 Our SPH model .....	23
4.2 Simulated conditions .....	24
4.3 Equilibration, simulation run and postprocessing .....	26
<i>5 Results and discussion</i> .....	27
5.1 Simulation and illustration .....	28
5.2 Reference simulation .....	29
5.3 Parameters effecting of the kinematic viscosity .....	32
5.4 Optimization directions .....	33
5.4.1 Problem statement .....	33
5.4.2 Suggested strategies for better control of viscosity .....	34
<i>6 Conclusions</i> .....	37
<i>References</i> .....	39

# List of Figures

Figure 1. Timeline of the use of predictive modeling and engineering in the food industry.....	9
Figure 2. Illustration of the axis multiscale modeling of the group MODIC.....	10
Figure 3. Multiscale modeling with the different spatial scales.....	12
Figure 4. (a) Principle of coarse-graining applied to a liquid (amorphous phase, e.g., monoatomic water) [8]; (b) CG of a peptide; (c) CG of a linear polymer[9] .....	13
Figure 5. Example of mapping (a)with Martini forcefield organic molecules[10] and (b)with Dissipative Particle Dynamics (DPD)[11]. .....	14
Figure 6. Different length and time scales and corresponding computational methods[35] .....	15
Figure 7. Schematic representation of molecular structures and the coarse-grained DPD models for (a) water, (b) CB particles, (c) AA molecules, (d) NMP molecules, (e) PVDF monomer, and (f) chemical structure of gelatin.[20] .....	16
Figure 8. Plot of the x-axis velocity profile of the particles at $y=0.5$ (at moment $t=t_{half}$ ) .....	22
Figure 9. SPH kernel scaled as used in our simulations, where dots represent the center of neighboring particles.....	24
Figure 10. Simulated domain and considered pair interactions. ....	25
Figure 11. Visualization of the flow tagging all particles close to the inlet (green color) at time 0 s, 0.1 s, and 0.5 s (see text for details) .....	28
Figure 12. (left) Comparison of simulated profiles with theoretical ones inferred from Eq. 3. for $t=0.0, 0.0002, 0.0005, 0.001, 0.002, 0.005, 0.01$ s and $v=0.001$ m/s (see text for details). (right) Radial distribution functions of SPH particles at $t=0$ and 0.2 s. The inset shows the tracking of SPH particles at the same times.....	30
Figure 13. Effects of the main studied parameters ( $U_0, d, q_1, c_0$ ) on the estimated kinematic viscosity (see text for details).....	33
Figure 14. Ensemble-averaged density and horizontal velocity as a function of the vertical position for the reference simulation. The same duration separates all profiles.....	34
Figure 15. (left) Curve of the relative velocity of the particles immediately adjacent to the moving plate as a function of simulation time and (right) magnified view of selected area in box. ....	35
Figure 16. Comparison of SPH simulations transient velocity profile to that of the analytical solution for of a Newtonian fluid being sheared with $c_0 = 0.4$ m/s. ....	36

**List of Tables**

Table 1. An overview of the apparent differences between MD, DPD, and SPH ..... 17

Table 2. An overview of the meshless simulation methods at the mesoscale (w/b = water/beads)  
..... 17

Table 3. Details of the work, which are included in the internship and reported. .... 19

Table 4. Reference values for the main objects of the parameterization ..... 25

# List of symbols

All units are SI.

$B = \frac{\rho_0 c_0^2}{7}$	constant in Eq. 4 [ $\text{kg}\cdot\text{m}^{-1}\cdot\text{s}^{-2}$ ]	$r$	radial distance [m]
$c_0$	speed of sound [ $\text{m}\cdot\text{s}^{-1}$ ]	$\mathbf{r}_{ij}$	vector connecting the centers of particles $i$ and $j$
$d$	gap thickness [m]	$R$	Hertz radius contact [m]
$D$	self-diffusivity [ $\text{m}^2\cdot\text{s}^{-1}$ ]	$t$	time [s]
$E$	Contact stiffness in Hertz contact repulsion force [N]	$u$	velocity defined in Eq. 3 [ $\text{m}\cdot\text{s}^{-1}$ ]
$f_{ij}$	The interaction forces between particles $i$ and $j$	$U_0$	velocity of the moving rigid beads (representing the moving plate) [ $\text{m}\cdot\text{s}^{-1}$ ]
$t^* = Fo = \frac{\nu t}{d^2}$	Fourier number [-]	$v$	velocity of a particle [ $\text{m}\cdot\text{s}^{-1}$ ]
$h$	smoothing length [m]	$W$	kernel weighted function
$k$	kernel radius [m]	$\gamma$	exponent in Tait's equation (see Eq. 4) [-]
$m$	mass of a particle [kg]	$\eta$	dynamic viscosity [ $\text{Pa}\cdot\text{s}$ ]
$P$	pressure [Pa]	$\nu$	kinematic viscosity [ $\text{m}^2\cdot\text{s}^{-1}$ ]
$q_1, q_2$	coefficients controlling the artificial viscosity term (Eq. 2)	$\rho$	density [ $\text{kg}\cdot\text{m}^{-3}$ ]

# Abstract

The report summarizes the first part of my M1 internship in the Modeling and Computational Engineering team of the UMR 0782 SayFood. The team develops a framework capable of simulating food deconstruction at several scales using mesoscopic Lagrangian descriptions of transport phenomena (rupture-dissolution, advection, mutual diffusion). Three coarse-graining techniques are part of the work. Mutual diffusion will be studied at the molecular scale in the second part of the work with Martini forcefield and Dissipative particle dynamics (DPD) at the molecular scale to preserve important chemical details and electric charges. The first part focused on flow problems involving DPD and SPH fluids, where SPH stands for Smoothed Particle Hydrodynamics. These techniques preserve momentum and have numerous appealing features, such as the capacity to treat naturally free surfaces and multiphase flows (emulsions, suspensions...). The nonlinear relationship between inputs and kinematic viscosity prevents shear velocities from being calculated correctly. A numeric Couette viscosimeter has been implemented to validate inputs and simulation strategies. The simulation includes a first equilibration to pack particles and an identification of the time scale to reach a steady state. The steps can be included in the simulation pipeline via the abstraction layer Pizza3.py for LAMMPS (<https://github.com/ovitrac/Pizza3/>) or replaced by its corresponding parameterization (involving many parameters including Reynolds and Mach numbers, particle size, the rigidity of Hertz contacts...) and that I contributed to implementing within a new class so-called generic (). The work was part of a Franco-American research project involving the group CARGILL and a British Ph.D. William Jenkinson.

**Keywords:** mesoscopic modeling, coarse-graining, viscosity, food, SPH, DPD, LAMMPS

# 1 Introduction

The Master 1 internship was carried out at INRAE (the French National Research Institute for Agriculture, Food and the Environment) in the group MODIC (Modeling and Computation Engineering) of the joint research unit 0782 research unit between AgroParisTech and INRAE. The subject treated essentially in technical terms cannot be separated from the team's research activity devoted to bridging atomistic and mesoscopic simulations. The front of science treated by the team is first presented before refocusing the presentation on the internship.

## 1.1 The research group MODIC

With high-performance and cloud computing development, modeling and simulation are thought to play an increasing role in almost all manufacturing activities. It is already involved in designing many high-tech products used in telecommunication, transportation, and chemical products. The case of the food industry and food products may look like an exception, and is it essential when agro-industrial products are very often associated with junk food? The success of *homo sapiens* as a biological species came from our capacity to feed and sustain its population and environment. The food industry is the leading manufacturing industry and the first industrial employer in developed countries. As shown in Figure 1, it has evolved rapidly during the last decades from a position where it was one of the first fossil fuel consumers (mainly for drying cereals, and sugar...) to converge progressively towards a unified approach linking sensory, nutritional, well-being, and health. Food engineering is the engineering branch supporting this evolution and integrated several advanced methods from other industrial domains, including membrane technologies and preventive approaches from the nuclear and aerospace industries. In return, some technologies such as extrusion processing and migration modeling of chemicals originate from the food transformation.



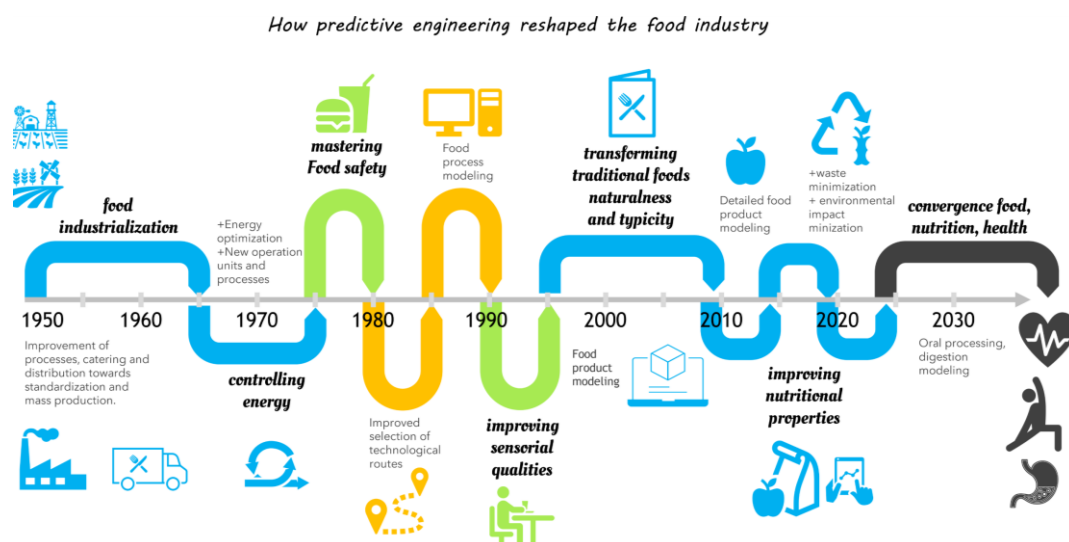
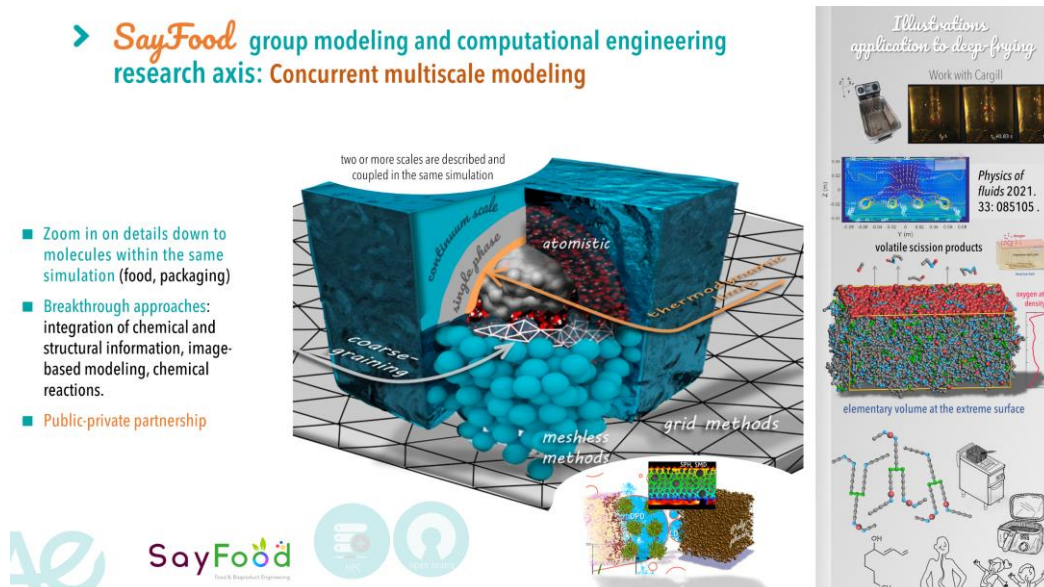


*Figure 1. Timeline of the use of predictive modeling and engineering in the food industry.*

*(Source: internal communication – Group MODIC, Olivier Vitrac)*

The group modeling and computational engineering (MODIC: MODélisation et Ingénierie par le Calcul) is a research group gathering chemical engineers, physicists, and mathematicians supporting the joint research unit Sayfood 0782 “*Paris-Saclay Food & Bioproduct Engineering*” (created in 2020 by merging two former research units of AgroParisTech and INRAE) in the exploration of new modes of food transformation (e.g., efficient industries, short supply chains, less packaging waste) and personalized foods (minimally-processed foods, protein substitution, food formulation for aged or allergic people, etc.). The group is also part of the Ile-de-France network in porous solids science RESPORE and its research axis (towards modeling at all scales). The emerging paradigm is multiscale modeling, where several scales are concurrently or sequentially at different scales. Indeed, foods are transformed to make objects (e.g., French baguette), but their final intent is to be deconstructed down to individual molecules and finally used as energy or building material by our bodies. The zig-zag molecules-food-molecules tremendously challenge modeling, particularly for the top-down branch (food deconstruction) following the first steps of food construction, conservation distribution, and final preparation.



(Source: internal communication – Group MODIC, Olivier Vitrac)

The right panel shows a recent application on modeling the flow and oxidation reaction kinetics within a deep-fryer both at the scale of oil bath (process scale) and molecular scale. Similar multiscale applications have been developed in the group for food packaging (not shown).

If food construction is essentially enthalpy-driven (work needs to be spent to create an ordered assembly), food deconstruction is, on the contrary, entropy-driven. The first step of deconstruction starts during the oral processing, and no mechanistic model can relate the initial micro and macrostructure with the mechanical response in the oral cavity. This problem is at the heart of a collaboration between the Cargill research center in Minneapolis (MN, USA) and the MODIC group, which is funding two doctoral theses. Additional projects, such as the project Assemblies funded by the French National Research Agency (ANR, in relationship with the unit Biopolymers Interactions Assemblies of INRAE in Nantes), address an unresolved question: how hydrophobic nutrients (e.g., vitamin A and antioxidants, or more negatively contaminants from the packaging) could be absorbed so efficiently from the food bolus in less than two hours (residence time in the small intestine). The simulation at the microscopic scale of the phenomena allows testing a hypothesis of mutual diffusion facilitated by the presence of bile salts which, more than solubilizing the fats, would modify the coefficients of water-oil partition.

## 1.2 Research objective

The physics of food obey soft matter [1] principles with their cohesion dominated by weak and non-covalent interactions: entangled polymers, self-organized colloids, and surfactants. Saliva and mechanical work contribute to overcoming the cohesive internal energy. Mesoscopic modeling offers the best compromise between preserving microscopic details (chemical details including local composition and supramolecular structures, phase organization) and continuum mechanics descriptions involving only effective properties. In food deconstruction, the assumptions of an effective medium are poorly verified: the interface quantities between phases increase considerably with fractal dimensions much greater than unity; the resulting properties vary with history, and the boundary conditions are essentially unknown. On the opposite side of the scale, simulations at the atomistic scale are not appropriate to study systems evolving far from thermodynamical equilibrium (*i.e.*, in the presence of mechanical stresses, gradients of chemical potentials).

Mesoscopic modeling is an umbrella encompassing a broad range of meshless techniques, including or not chemical details. They are promising as they could potentially fill the gap between a continuum description of foods and their constituents. The study focuses on the parameterization of mesoscopic simulations to describe solid-fluid interactions during oral treatment and the mutual diffusion associated with interactions between self-assembled bile micelles of ~5 nm in diameter and a fat globule after emulsification in the small intestine.

## 1.3 Document outline

The construction of the report was a matter of choice and compromise. Two techniques are used: SPH (smoothed particle hydrodynamics) and DPD (dissipative dynamics). The report was written in the middle of the internship, starting on April 15. The two techniques have been reviewed and are presented in section 2. The aim is to show that although they are applied at very different scales, they have a relatively similar origin, formalism, and implementation. However, section 3 only presents the objectives of the technique that has been the most used in SPH, which corresponds to the direct collaboration with William Jenkinson, Ph.D. student of the MODIC team. The results are presented and discussed in section 4. Their generalization on a smaller scale and the possibility of combining the two techniques in the same simulation on both sides of the thermodynamic equilibrium are discussed in the last section, “conclusions and perspectives.”

## 2 Short review of meshless simulation methods at mesoscale

Mesoscopic simulation is a set of Lagrangian representations (*i.e.*, explicitly integrated trajectory simulations) that involve particles instead of meshes. Since the corresponding techniques are not part of the conventional background of chemical and mechanical engineers, this review was essential to familiarize me with the bestiary of concepts and implementations. They occupy the gap between classical molecular dynamics simulation methods and finite element/volume techniques. They have various foundations, but they share a common point: their ability to be efficiently deployed in classical molecular dynamics codes. The ability to link time and length scales within the same software [2] and concurrently [3] was a dream and rapidly became an active research field.

### 2.1 What is the mesoscale

The definition of mesoscale is not rigid, and it is a relative concept between microscale and macroscale, which is used in many fields, such as computational fluid dynamics, computational chemistry, computational material science, computational physics, and computational mechanics. Multiscale models are defined as a hierarchy of interconnected sub-models which describe the material behavior at different spatial scales[4]. The critical challenge in multiscale computer simulation consists of developing the concepts and algorithms that link the different length and time scales controlling the evolution of complex systems.

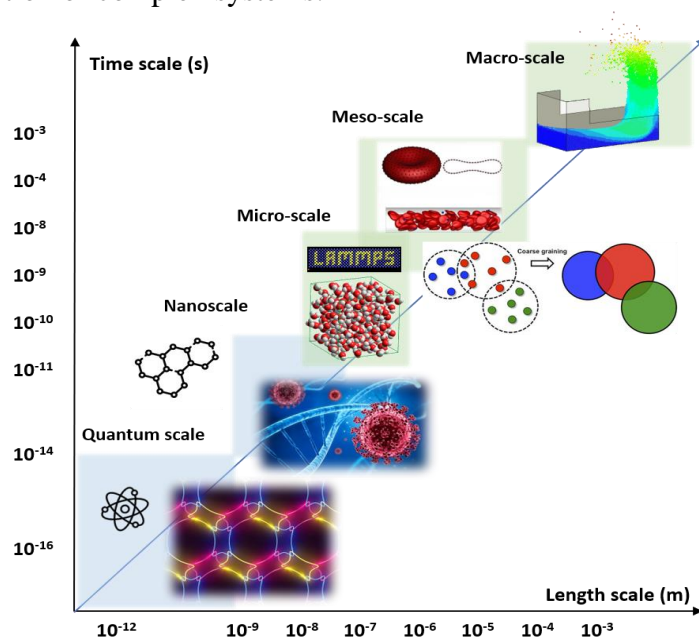


Figure 3. Multiscale modeling with the different spatial scales

(Source: Author's image)

First, for the “microscale” (a characteristic length ranging from  $10^{-8}$  to  $10^{-6}$  m and a characteristic time ranging from  $10^{-11}$  to  $10^{-8}$  s), it is capable of behaving at the electronic and atomic levels, which encompasses the nature of chemical bonding and all relevant atomic-level processes and mechanisms. Secondly, the level generally defined as “mesoscale” emphasizes the critical role played by the microstructure of materials, for example, colloidal systems and multiphase flows in porous media, migration of the cells normal to the wall of the vessel, and the formation of the cell-free layer[5]. In computational material science and computational mechanics, mesoscale usually involves a characteristic length ranging from  $10^{-7}$  to  $10^{-4}$  m and a characteristic time ranging from  $10^{-9}$  to  $10^{-3}$  s. Finally, the results of the “mesoscale” simulations provide the basis for a continuum description of the material and thus enable macroscale simulations (a characteristic length bigger than  $10^{-4}$  m and a characteristic time bigger than  $10^{-3}$  s), for example, in the form of a finite element or phase-field approach.

Mesoscale modeling, also called coarse-grained (CG) modeling, is a technique aiming to reduce the number of degrees of freedom and, therefore, the number of pair interactions ( $N^2$  speedup with the number of particles  $N$ )[6]. Hardcore interactions (repulsive forces) dominate at the atomistic scale and are responsible for large excluded volumes. In CG models, softcore dominate and enable particle/bead overlapping. Though CG can be viewed as low-resolution models [7], they require new potentials or forces, which cannot be defined uniquely. As an illustration of accessible gains, dropping hydrogen atoms and 1-to-4 mapping of heavy atoms increase integration time steps up to  $5\text{-}20 \times 10^{-15}$  s instead of  $0.5\text{-}1 \times 10^{-15}$  s.

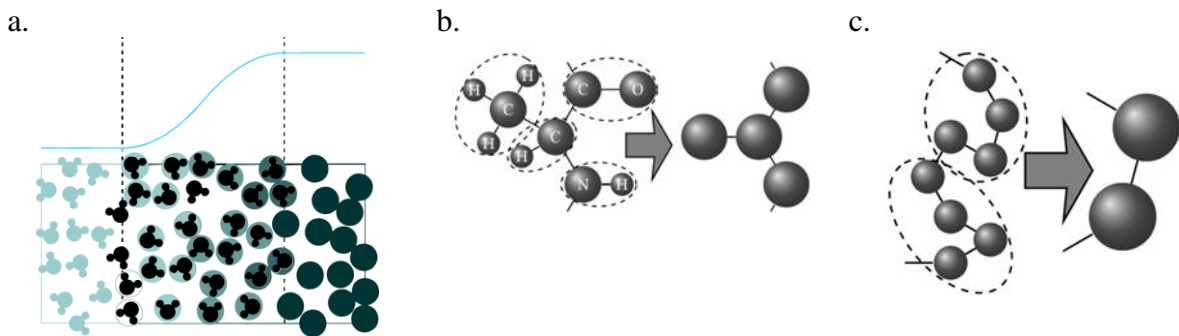


Figure 4. (a) Principle of coarse-graining applied to a liquid (amorphous phase, e.g., monoatomic water) [8]; (b) CG of a peptide; (c) CG of a linear polymer[9]

## 2.2 Coarse-graining modeling methodology

Coarse-graining (called CG below) can be classified into three categories[10]: (a) by the theory of mechanical statistical equilibrium, the integration of CG is carried out using the “time average” and the “ensemble average.” (b) according to the statistical mechanical theory of transport processes, the corresponding force field is used to complete the coarse-graining. (c) CG through by assuming that the crystal is homogeneously deformed.

Most of the CG modeling for soft matter are based on the reduced-structure approach. First, this approach reduces the structure directly by simplifying several atoms into a rigid CG particle. Then, it needs to build a suitable force field to match the CG model properties (such as the structure, thermodynamic properties and forces) with the underlying atomistic model.

As an example of a popular CG force field, the Martini model has been found more and more applications in the field of materials science. It typically gathers four non-hydrogen atoms in a CG particle, as shown in Figure 5. The underlying assumption of the Martini method is that the thoroughly parameterized properties of individual Martini bead types can be transferred to the molecule as a whole when they are linked together to reproduce the overall topology of the desired molecule. This basic assumption also poses some pitfalls[29], so comparisons with higher resolution atomic simulations or experimental data are often required[30].

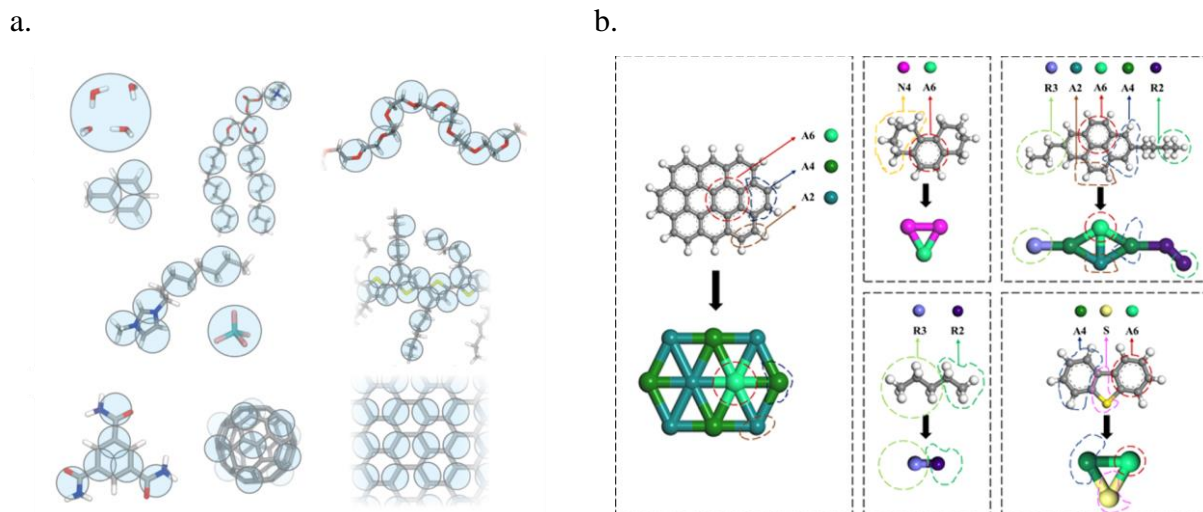


Figure 5. Example of mapping (a)with Martini forcefield organic molecules[10] and (b)with Dissipative Particle Dynamics (DPD)[11].



## 2.3 Specific techniques in multiscale modeling

Large quantities of computational models are proposed for coping with the limitations on different scales (as shown in Figure 6). In microscale, classic molecular dynamics (MD) has been in development for a long time and provides a clear fundamental path to understanding the behavior between atoms in the fluid flow. However, the time and length scales of the models are so small that the resulting detail can make modeling very expensive.

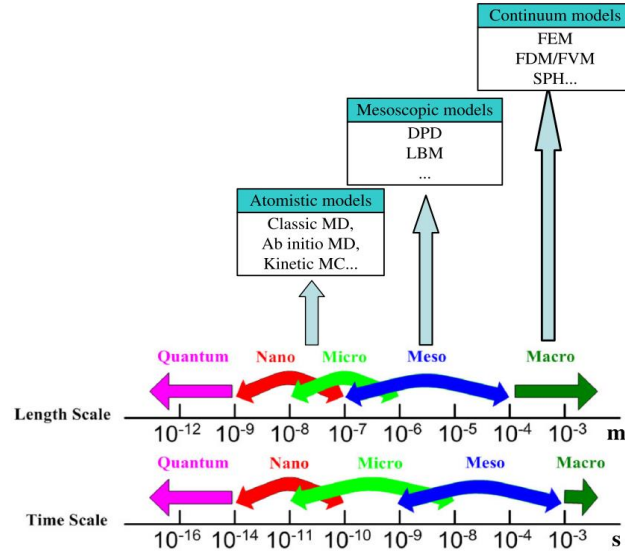


Figure 6. Different length and time scales and corresponding computational methods[35]

In mesoscale, dissipative particle dynamics (DPD), similar to the MD model, was developed based on a coarse-grained approach, that small atomic or molecular clusters in microscopic regions become continuous solids or fluids by replacing a unit volume of fluid with particles. DPD facilitates the simulation of physically interesting and complex fluid systems and focuses more on the structure of molecules than on their atomic composition, and is therefore superior to MD on longer time scales and larger length scales. While DPD is not as computation- ally efficient as lattice Boltzmann simulations, it is a more flexible method that does not suffer from the numerical instability associated with many lattice Boltzmann applications[35].

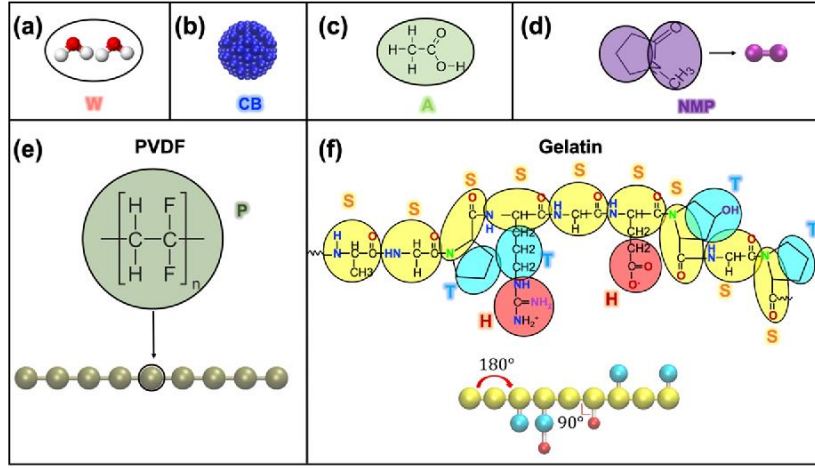


Figure 7. Schematic representation of molecular structures and the coarse-grained DPD models for (a) water, (b) CB particles, (c) AA molecules, (d) NMP molecules, (e) PVDF monomer, and (f) chemical structure of gelatin.[20]

The Smoothed Particle Hydrodynamics (SPH) technique was pioneered in the 1970s by Gingold, Monaghan and Lucy[21][22] for applications in astrophysics, but the 1980s and 1990s saw its extension to more human-scale problems such as shock dynamics [23], free-surface flows [24], and viscous and porous flows[25]. The method is part of an active research field and comes with several strengths and weaknesses compared to conventional mesh-based modeling methods. A thorough discussion on the current weaknesses of SPH can be found in [26], but to summarize common grievances for those coming from mesh methods such as FEM and FVM include [27]:

- low convergence, consistency, and stability,
- difficulties prescribing wall boundary conditions, particularly flow inlets/outlets,
- difficulties in dealing with variable space resolutions, and achieving some analogy to the adaptive meshes.

The method's strengths come from its ability to simulate continuum mechanics with a Lagrangian physics that more readily describes large deformations and interfaces than conventional mesh-based methods. This has drawn interest to the method from those in the food research community looking to solve problems unaddressed by conventional numerical methods [28].

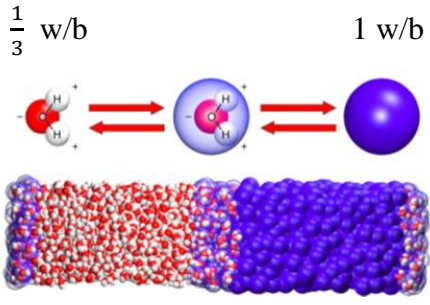
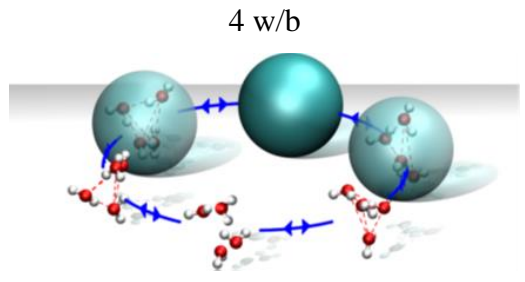
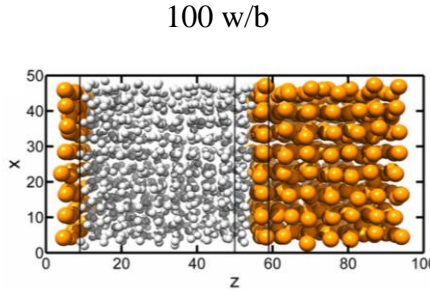
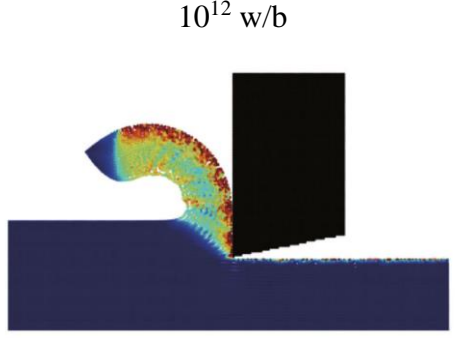
At the macroscale, the SPH particle approximation converts the continuous form of the kernel approximation of a field function and its derivatives to the discrete summations over a set of particles[36]. It makes the SPH method simpler by dispensing with the need to use a background grid for numerical integration. As a particle-based method, SPH is very much similar to MD and DPD. These three particle-based methods have the same characteristics: they are all purely lattice-free particles and can operate under Lagrangian properties. These three methods can therefore be



Table 1. An overview of the apparent differences between MD, DPD, and SPH

	Scale	Newton's second law use...	A particle is regarded as...
<b>MD</b>	micro-scale	potential function	a single atom or molecule
<b>DPD</b>	meso-scale	weight function	a small cluster of atoms or molecules
<b>SPH</b>	macro-scale	smoothing function	a very small region

Table 2. An overview of the meshless simulation methods at the mesoscale (w/b = water/beads)

 <p><b>Hardcore interactions = classical MD</b> (no-overlap)[30]</p>	 <p><b>Soft-core interactions = DPD</b> (small overlaps)[31]</p>
 <p><b>SDPD[32]</b></p>	 <p><b>SPH (large overlaps)[33]</b></p>

linked together in specific cases and give rise to other derivative methods (e.g., SDPD). At the same time, they complement each other and thus correspond better to physical properties at multiscale.

## 2.4 Intermediate summary

The previous two sections introduced the ambition of the group MODIC and justified the choice of techniques chosen by the group to be part of a unified numerical framework. My internship includes the use of both DPD and SPH methods. The team will take advantage of its results to link the two approaches within the Pizza3 code under development (see §3.3), which I used and modestly contributed to extending. As the internship is currently only halfway through, the sections following in this report only cover only the use of SPH. (See Table 3)

## 3 Goals and approaches

### 3.1 Work plan: intermediate and final goals

The internship involves two coarse-graining techniques, which have been organized to accommodate current research priorities and the move of the cluster of computers to the new campus Agro of the University of Paris-Saclay this summer. Intensive computations on the cluster have been scheduled before the move. The remaining activities can be carried out on workstations. The considered works (done or planned) during the internship are shown in *Table 3* and are built around a variation of the same problem: how to build a mesoscopic simulation of process transport without a mesoscopic theory. As justified earlier by Irwing and Kirkwood [13] for hydrodynamics, exact theories involve quadrature of densities in the configuration space of pair molecules. This information is lost during the coarse-graining process, and particles represent many molecules regardless of their true configurations.

The first part of the internship, which is part of the results presented, is focused on the parameterization of the kinematic viscosity in an SPH simulation for a liquid with Newtonian behavior (water, oil). It is evident that an SPH particle carries too many molecules to describe molecular diffusion; these aspects will be studied in the second half of the internship by using simulations already performed by the team. The SPH method is not free of problems, even if it can be seen as a collocation method for solving the Navier-Stokes equations (i.e., without any molecular theory). It involves central (radial) forces and does not allow friction between particles or impose any transport coefficient. In the vicinity of solid particles, which force a particle interpretation (and are no longer probabilistic) and impose only radial forces at fluid-solid and solid-solid interfaces (Hertz contacts), the emergence of the concept of viscosity from such simulations and the prevention of flow slipping constitute the core of the work.

The prioritization of the SPH method over other work by the team is justified because, in a multiscale multi-method food deconstruction simulation, the SPH method will transport food on the largest scales (i.e., throughout the digestive tract). Other smaller-scale methods will provide details, mixing at interfaces, and interactions with the micellar phase at the nanoscale. The interaction between all these scales is likely the key to understanding the extreme effectiveness of our digestive system in separating and trapping food components in a specific way.

Table 3. Details of the work, which are included in the internship and reported.

Technique and context	Contribution	Reported results
<b>Parameterization SPH to simulate laminar flows with controlled viscosity.</b>	<p>The group wanted to offer a minimum parameterization of viscosity in the abstraction layer Pizza3.py</p> <p><b>Role:</b> development and validation of a virtual viscosimeter to set viscosity model in Pizza3.py</p>	The core of the reported results
<b>DPD is a generic tool to simulate out-of-equilibrium mass transfer and flows. The intent is to compare DPD with detailed simulations (Martini) and coarser ones (SPH).</b>	<ul style="list-style-type: none"> <li>• Same work as above with a DPD forcefield (done in previous works)</li> <li>• Simulating a DPD fluid (water) to match</li> </ul> <p><b>Role:</b> generating DPD fluid with the abstraction layer Pizza3.py for LAMMPS, preparing concurrent simulation of DPD and SPH with Pizza3.py.</p>	To be initiated only in the second part of the internship.
<b>Classical molecular dynamics using the Martini forcefield (ongoing work within the project ANR Assemblies) to preserve enough details to simulate mutual diffusion, including bile salts using the Kirkwood-Buff theory [14]</b>	<ul style="list-style-type: none"> <li>• The forcefield for bile salts and vitamin A has been validated by previous works.</li> <li>• Simulations were launched and collected before my arrival.</li> </ul> <p><b>Role:</b> calculating Kirkwood-Buff Integrals (KB I), van Hove correlation functions, and concentration profiles to interpret mutual mass transfer (triacylglycerols, phospholipids, vitamin, bile salt, water) is pending.</p>	To be initiated only in the second part of the internship.

### 3.2 Main goals

In simulations at equilibrium involving statistical ensembles, the transport coefficients can be inferred from the long-time integral of the autocorrelation function of fluxes (mass or momentum)[15]:

$$D = \int_0^\infty \langle \mathbf{v}(t) \cdot \mathbf{v}(0) \rangle dt, \text{ self-diffusion } (\mathbf{v} \text{ is the velocity and } 0 \text{ any initial time})$$

$$\eta = \rho v = \frac{v}{k_b T} \int_0^\infty \langle P_{xy}(t) \cdot P_{xy}(0) \rangle dt, \text{ viscosity (here from 2D simulation)} \quad \text{Eq.1}$$

$$\text{with } P_{xy}V = \sum_{i=1}^N m \dot{x}_i \dot{y}_i + \frac{1}{2} \sum_{j \neq i} y_j F_j^{(x)}, \text{ pressure tensor (here along } xy)$$

Eq.1 relies only on statistical mechanics principles and demonstrates that there is no natural way to force a given viscosity as it originated from the diffusivity of momentum or equivalently from the decorrelation time of the pressure field. It is an emerging property and not the cause of the displacement of particles. The same comment holds for diffusivities. The SPH formulation

proposed by Monaghan incorporates an artificial viscosity,  $\mu_{ij}$ , derived from the formulation firstly suggested by Von Neumann and Richmyer at Los Alamos to describe shockwaves met during the Manhattan Project[16]. The formalism combined with adequate solid particle definition may offer a potential strategy to control the propagation rate between particles. Shockwaves are associated with length scales comparable to a few molecular mean-free paths and, therefore, much smaller than SPH particles. They are usually simulated as Hugoniot conditions, with discontinuous property jumps. The original approach adds a dissipative term  $-q_2 \rho h^2 \frac{\partial v_x}{\partial y} \left| \frac{\partial v_x}{\partial y} \right|$  which is positive in compression and negative in tension, with  $q_2$  a constant. This term controls the dilatational viscosity, also-called bulk viscosity. Landshoff added a linear term which linear with the velocity gradient  $\frac{\partial v_x}{\partial y}$  (here in 1D) and scales as  $q_1 \rho h c_0 \frac{\partial v_x}{\partial y}$ , where  $q_1$  is a constant and  $c_0$  is the local speed of the sound. The characteristic length  $h$  should be chosen commensurable to the particle size to dampen the shock rapidly and keep the jump inside the particle.

Monaghan[17] implemented the viscosity as a normal force opposing the encounter of two particles and oriented along the line connecting the centers of particles  $i$  and  $j$ , denoted  $\frac{\mathbf{r}_{ij}}{\|\mathbf{r}_{ij}\|}$  with  $\mathbf{r}_{ij} = \mathbf{r}_i - \mathbf{r}_j$ . The resulting radial force acting on the particles in the range of a weighted kernel ( $W$ ) reads (when  $(\mathbf{r}_i - \mathbf{r}_j) \cdot (\mathbf{v}_i - \mathbf{v}_j) < 0$ ):

$$\begin{aligned} \mathbf{F}_{ij}^v &= -v_{ij} \frac{\partial W}{\partial r} \bigg|_{r=r_{ij,h}} \frac{\mathbf{r}_{ij}}{\|\mathbf{r}_{ij}\|} \\ v_{ij} &= \frac{1}{\langle \rho_{ij} \rangle} (-q_1 c_0 \mu_{ij} + q_2 \mu_{ij}^2) \\ \mu_{ij} &= \langle h_{ij} \rangle \frac{(\mathbf{r}_i - \mathbf{r}_j) \cdot (\mathbf{v}_i - \mathbf{v}_j)}{r_{ij}^2 + 0.01 \langle h_{ij} \rangle^2} \end{aligned} \tag{Eq. 2}$$

with

In other words,  $v_{ij}$  generates a repulsive force when the particle  $i$  approaches (the distance is reduced)  $j$  to prevent the collision (in fact, to mimic the shock). The repulsion is low when the particles move in the same direction and much higher when the particles move in the opposite direction. The linear viscosity term is proportional to the product between  $q_1$ ,  $c_0$ , and  $h$  or its average  $\langle h_{ij} \rangle$  when particles have different sizes. At this stage, it is worth noticing that  $c_0$  is not the real speed of the sound but an artificial one chosen so that the simulation remains subsonic but with a value high enough to enable pressure to cross a distance commensurable to  $h$  during an integration time step. Morris[25] suggests choosing a Mach number close to 0.1 based on the velocity of the fastest particle.

### 3.3 Approaches followed

The group MODIC uses the classical molecular dynamics code LAMMPS (Large-scale Atomic/Molecular Massively Parallel Simulator) from Sandia Laboratories (USA)[2] as a “universal” computational engine for very different physics, so-called internally “frameworks.” This approach takes the benefit of the many user packages available, which can be compiled statically with LAMMPS (more than 1 million lines of C++ code) and run in parallel either on workstations (running on Linux Ubuntu 18.04) for debugging or on the cluster (running on Linux CentOS 8.x) of the research unit. The interactions with the LAMMPS engine occur via an input script (sharing some similarities with Tcl). Instructions and commands are executed sequentially, each running in parallel on many processors (from 1 to several million) from a shared variable space. The group MODIC works on developing an abstraction layer in Python 3.x (Pizza3.py)[18] enabling the combination of different frameworks within the same environment. For the end-user, the apparent advantage is the coding through a syntactic front-end in object-oriented Python offering sub-classes to manage data, pipelines, templates, and static execution (duplication, factorization, inheritance from previous scripts or simulations, simulations restarts) at all stages: drawing/design, input files generation, execution, and post-treatment. Almost all my work was carried out with Pizza3.py, for which I contributed to developing a high-level class, so-called “generic,” enabling users to encode real fluids (Newtonian for now) into SPH-like and DPD-like fluids. The top class has been called *generic* (). No prior knowledge of LAMMPS or LAMMPS pragma is required to use *generic* () and Pizza3.

A validation of fluids (defined by the size) is proposed by testing the SPH-liquids in a virtual Couette viscosimeter. This step can be inserted in the simulation flowchart before production or used to tabulate a priori a viscosity model. Inside flows created by pushing a fluid (moving object), pressure, or a release of potential energy (*e.g.*, Torricelli’s experiment), the time scale is imposed by the flow rate, momentum conservation, and gravity acceleration, respectively. In dissipative flows, the time scale originates from dissipation/relaxation and is governed by the kinematic viscosity and the solid-fluid interactions (fluid-walls, fluid-floating, or in suspension). In our SPH simulations, that is to say:

- the absolute and relative size of the fluid, solid particles ( $r$ ,  $r_{ij}$ ),
- the kernel and its smoothing length ( $h$ ),
- the rigidities of the contact between fluid-solid particles ( $E$ ),
- the dimensions of channels,
- the speed of the sound ( $c_0$ ),

- the Reynolds number ( $Re$ ),
- the size of the system and periodic boundary conditions.

Additional factors, such as the density and type of particle packaging (triangular, square, and hexagonal in 2D dense packing, face-centered cubic, and hexagonal close-packed in 3D dense packing) can also affect the result. This problem originates mainly from the non-physical nature of the initial packing. Pizza3.py resolves the problem by implementing equilibration steps against normal or shear forces. These first steps minimize the system's internal energy before introducing an external disturbance.

Contrarily to real viscosimeters, there is no easy manner to recover shear stress or torque from SPH or DPD simulations (see the discussion in Ref.[19]). Viscosity was reconstructed from the time required by the system to reach a steady state. The dimensionless analytical solution for 2D Couette flow is given by Lucy [22]:

$$u^*(t^*, y^*) = 1 - y^* - \frac{2}{\pi} \sum_{n=1}^{\infty} \exp(-n^2 \pi^2 t^*) \sin(n \pi y^*) \quad \text{Eq. 3}$$

Where  $u^* = \frac{u(y,t)}{U_0}$ ,  $y^* = \frac{y}{d}$ ,  $t^* = \frac{\nu t}{d^2} = Fo$  (or Fourier number), the velocity of the moving plane is  $U_0$ , and the gap distance is  $d$ . In the implemented protocol, the kinematic viscosity is inferred from the half-time  $t_{1/2}$ , so that  $u^*(t_{1/2}^*, y^* = \frac{1}{2}) = \frac{1}{4}$ , with  $t_{1/2}^* = \frac{t_{1/2} \nu}{d^2} \approx 0.094686959568062$ . This condition guarantees that the disturbance propagated across the thickness. For strictest validations (Newtonian flow, constant and uniform viscosity), the simulated velocity profiles were compared directly with Eq. 3.

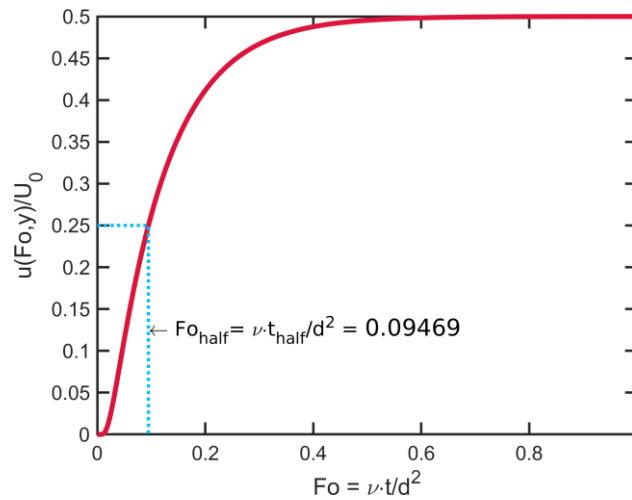


Figure 8. Plot of the x-axis velocity profile of the particles at  $y=0.5$  (at moment  $t=t_{half}$ )

## 4 Methodology

### 4.1 Our SPH model

The force acting on the particle due to pressures is computed by approximating the pressure gradient from both the weighting kernel  $W$  and a simple Equation of State (EOS):

$$\frac{d\mathbf{v}_i}{dt} = - \sum_{j \text{ neighboring } i} m_j \left( \frac{P_j}{\rho_j^2} + \frac{P_i}{\rho_i^2} \right) \frac{\partial W}{\partial r} \bigg|_{r=r_{ij},h} \frac{\mathbf{r}_{ij}}{\|\mathbf{r}_{ij}\|} \quad \text{Eq. 4}$$

with  $P = B \left( \left( \frac{\rho}{\rho_0} \right)^\gamma - 1 \right)$ , Tait's equation (EOS)

where  $P$  is pressure. For a weakly compressible approximation of a fluid may use  $\gamma = 7$ .  $B$  is some constant scaled by the speed of sound,  $c_0$ , conventionally chosen equal to  $\frac{\rho_0 c_0^2}{7}$  with  $\rho_0$  the targeted fluid density. This later formulation is weakly compressible SPH (WCSPH) and appropriate to simulate liquids.

Using the collocation properties of SPH kernels, volume integrals are replaced by simple sums. The mass balance around the particle  $i$  estimates the density at its center:

$$\rho_i = - \sum_{j \text{ neighboring } i} m_j W(|\mathbf{r}_i - \mathbf{r}_j|, h) \quad \text{Eq. 5}$$

where the density of  $i$  is evaluated as  $\rho_i$  and is related to the value of the mass of all the neighbors,  $m_j$ , and weighted by the kernel  $W$ . The following cubic kernel was used with a graphical interpretation shown in Figure 9:

$$W(r, h) = \frac{12}{\pi h^3} \begin{cases} \frac{2}{3} - q^2 + \frac{1}{2} q^3 & 0 \leq q \leq 1 \\ \frac{1}{6} (2 - q)^3 & 1 \leq q \leq 2 \\ 0 & q > 2 \end{cases} \quad \text{Eq. 6}$$

where the  $q = \frac{2r}{h}$  is the ratio of the distance between any two particles to the smoothing length.

The concept of pseudo-viscosity was implemented as Eq. 3.

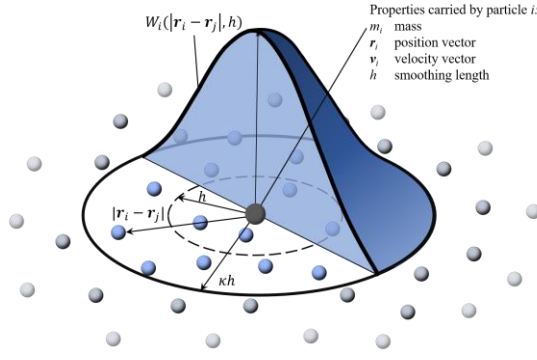


Figure 9. SPH kernel scaled as used in our simulations, where dots represent the center of neighboring particles

## 4.2 Simulated conditions

The Couette viscometer was modeled in pseudo 3D as three regions as illustrated in Figure 10. Pseudo 3D means that the thickness ( $z$  direction, not shown) of the plane is commensurable to the particle diameter. Periodic boundary conditions enable the particles to move along  $z$ . Additional periodic conditions are applied along  $x$  to enable a continuous horizontal displacement of particles. Top and bottom regions were made with rigid particles interacting with SPH particles in the central region through Hertz contacts (repulsive forces, see interpretation in Figure 10):

$$f_{ij} = E \sqrt{(r_{cut} - r) \frac{R_i R_j}{r_{cut}}} , \quad r < r_{cut} \quad \text{Eq. 7}$$

$$\text{with} \quad r_{cut} = R_i + R_j$$

where  $E$  is the contact stiffness, which has units of pressure ( $10^{12}$  Pa was applied).



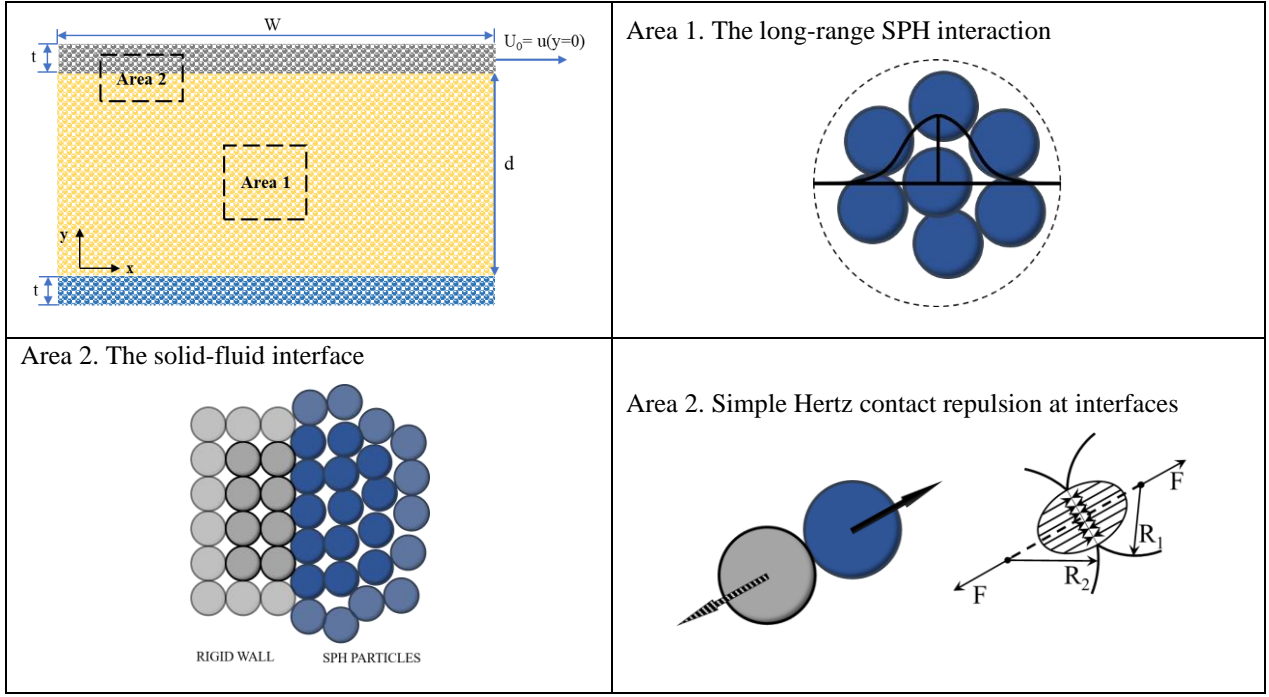


Figure 10. Simulated domain and considered pair interactions.

The reference conditions are listed in Table 4. They correspond in the context of oral processing of what could be expected for thin film of saliva maintained between the tongue and the palate. The targeted kinematic viscosity determinations are expected to be range between  $10^{-6}$  (water) and  $10^{-4}$  (oil)  $\text{m}^2 \cdot \text{s}^{-1}$ . For the reference condition, the gap contained 100 SPH particles vertically and 100 SPH particles horizontally for a total of 11899 particles (SPH and rigid ones).

Table 4. Reference values for the main objects of the parameterization

Parameter	Description	Reference value	Units
$U_0$	Velocity of the moving plate	0.001	m/s
$d$	Distance between the walls	0.001	m
$h$	Smoothing length	$1 \times 10^{-5}$	m
$c_0$	Speed of the sound	0.2	m/s
$q_1$	Coefficient of the viscosity term	50	

### 4.3 Equilibration, simulation run and postprocessing

As a particle method with particles of a fixed size, a simple space filling model was used to generate the geometries. As such the initial particle configuration may generate large forces as an artifact of this model. An equilibration (or relaxation) step was introduced to dissipate these forces and allow the system to reconfigure. From there initial configuration, pre-shearing phase repacked the particles, particularly at the wall, to a more stable arrangement. The velocities of the particles were then steadily reduced to remove kinetic energy from the system until it was in a relaxed, quasi-static state, from which the simulation run was launched.

All simulations were run in parallel on a 256-core processor node using the SPH implementation of the SMD user-package of the LAMMPS code (<https://www.lammps.org/>). LAMMPS scripts and particle data files were generated via the abstraction layer Pizza3.py (<https://github.com/ovitrac/Pizza3/>). A typical job was ran between 10 and 20 minutes on 32 and 16 cores.

Postprocessing was achieved through a combination of Ovito (<https://www.ovito.org/>) for visualization and per-simulation data analysis, and Pizza3.py for batch data analysis.

## 5 Results and discussion

This section reports the results obtained from April 15<sup>th</sup>-June 15<sup>th</sup> and related to the parameterization of kinematic viscosity,  $\nu$ , for SPH simulations (Lagrangian descriptions). The reader should be aware that SPH fluids do not verify common properties implemented with continuum mechanics principles in Eulerian approaches (finite element or finite volume approaches):

- Only two types of particles are considered: updated Lagrangian for the liquid and rigid for the walls.
- The concept of friction does not exist in SPH fluids (only radial forces are centripetal or centrifuge); it is inherent to molecular dynamics- (MD) like approach.
- SPH fluids remain partly compressible, and density fluctuations propagate as waves even at a steady-state; pressure is defined through an equation of state (Tait's equation).
- SPH fluids interact with rigid walls through Hertz contacts without adhesion; walls are not made with SPH particles (with zero or fixed velocity) as the intent was to estimate wall shear stress in more general cases (e.g., around objects)
- The interactions between SPH and rigid particles force the SPH particles to behave as hardcore particles instead of as blurred ones (the SPH kernel does not hold for these interactions); the final aim is to parameterize with very different particles (updated and total Lagrangian, rigid...).

The results obtained with our *in-silico* viscosimeter are presented comprehensively in four parts. The first part illustrates how momentum is transferred qualitatively from a wall made with rigid particles (see Figure 11) to an SPH fluid. Rigid and SPH particles have the same diameter. The second sub-section shows how kinematic viscosity was estimated from the time to reach a velocity equal to  $U_0/4$  in the central plane one-quarter of the channel. According to Eq. 3, this time is theoretically independent of  $U_0$ , but the distance travelled by the beads depended on  $U_0$ . In other words, beads need to translate on a larger distance when  $U_0$  is larger. The third part discusses the main parameters affecting viscosity. Finally, the directions of improvement based on this explorative study are proposed in the last section. For each part, a mechanistic interpretation is suggested.

## 5.1 Simulation and illustration

SPH particles are between 1 billion and 1 trillion heavier than DPD ones, therefore not subjected to strong accelerations and carrying much larger momentums. Figure 11 illustrates the displacement of tagged beads (in green) provoked by the displacement of the top wall at a velocity  $U_0$  is 0.001 m/s. The particle diameter is  $10^{-5}$  m. All conditions are similar to the reference conditions listed in Table 4, except the factor  $q_1$  which has been set to 5 instead of 50. This condition enabled a fully developed linear profile when the SPH particles in contact with the top surface translated more than half the length of the channel, which is 0.5 mm. The periodic boundary conditions along the horizontal axis allowed the flow from right to left. A periodic boundary condition is also applied perpendicularly to the channel to enable the use of spherical kernels. Though it may be counterintuitive, the SPH particles follow the wall particles in the absence of attractive forces or friction forces at the surface of each particle (see the interpretation of Hertz contacts in Figure 10 (bottom left)). Similarly, the particles in contact with the bottom wall (immobile) do not translate even when the steady-state is reached. The steady-state condition corresponds theoretically to the same relative horizontal velocity for all SPH particles adjacent along  $y$ . It was visualized by the linear distribution of tagged SPH particles.

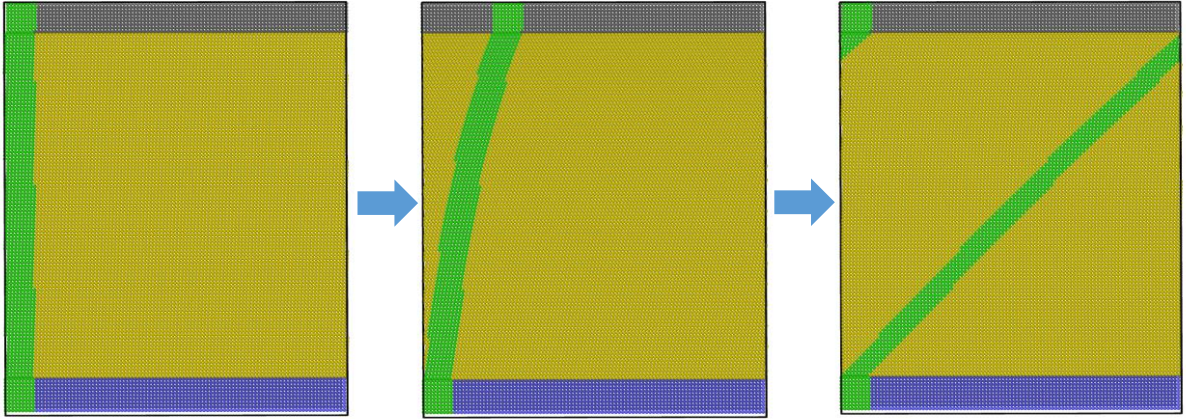


*Figure 11. Visualization of the flow tagging all particles close to the inlet (green color) at time 0 s, 0.1 s, and 0.5 s (see text for details)*

### *Mechanistic interpretation*

At this stage, it should be noted that no hydrodynamic theory applies between the rigid plate and the SPH particle, only momentum propagates spread from top to bottom, which can be characterized by the kinematic viscosity. Just as diffusion coefficients do not explain the translation of molecules, viscosity does not explain the viscosity gradient; it can only describe it. The distribution of tagged particles will stretch endlessly without any stable pattern even at steady state

(Lagrangian description). The particles will “slide” on top of each other; particles on top will eventually double all the particles in a lower position. Horizontal momentum propagates from bottom to top between a source and a sink, respectively, between the rigid particles of the upper wall in translation and the rigid particles of the immobile lower wall. As the permeation of matter through a membrane, a steady-state is established, but the particles continue to move. Momentum is transported via “smooth collisions” (encounters) between particles in all directions. Only a net momentum transport exists from top to bottom.

Since the kernel's support is 1.5 times the diameter of the particles (see Figure 10 ), SPH particles are expected not to be too sensitive to the packing. An initial square packing is applied before the initial equilibration step. The equilibrium is performed by applying pressure from the top. It does cause visible displacements of particles but enables the simulation to start with uniform Hertz contacts with rigid wall particles, including across the periodic boundaries. No external force is applied except gravity (applied along  $y$ ) when the top wall is moved. It was a deliberate choice not to use an initial hexagonal packing because it minimizes the number of contacts between an SPH particle and a rigid particle (one instead of two). The resulting force has a vertical component essentially. The fluid motion is not preconfigured; the described situation is the worst case. It is important to note that the velocity gradient is not well defined for the SPH particles in contact (gradients are radially distributed due to spherical kernels). The results in Figure 11 Figure 11. Visualization of the flow tagging all particles close to the inlet (green color) at time 0 s, 0.1 s, and 0.5 s (see text for details) show that the SPH layer in contact has a natural tendency to follow the rigid one. This effect was sought as it avoids coating all the rigid objects with an SPH layer, which should move together with the rigid objects (walls, suspensions). A more detailed analysis will follow to understand the origin of the translational motions as observed.

## 5.2 Reference simulation

As previously stated, the physics of SPH fluids deviated from fluid definitions derived from continuum mechanics. The SPH technique behaves as a reasonable collocation method for the layers, not in contact with the rigid walls. Conversely, the extreme top and bottom SPH layers behave as repulsive particles for their interactions with rigid ones. Other deviations such as the roughness of the surface make the simulations different from the standard transient Couette (TC) problem. However, analytical solutions to the TC problem offer a practical framework to estimate the apparent kinematic viscosity from simulations. The simulated velocity profiles corresponding

to the reference conditions (see Table 4) are compared with theoretical ones in Figure 12. The corresponding  $Fo = t^* = \frac{vt}{d^2}$  values were inferred by estimating  $t_{1/2}$  from the ensemble-averaged velocity along the central line. The resolution in time was enhanced by interpolating the averaged velocity with a Hermite polynomial between recorded frames (more than 200 frames were used), as shown in §3.3. The estimated value of kinematic viscosity was of  $4.5 \times 10^{-5} \text{ m}^2/\text{s}$ . The simulated profile for  $Fo=0.08927$  was the closest of  $Fo_{1/2} \approx 0.0946$ .

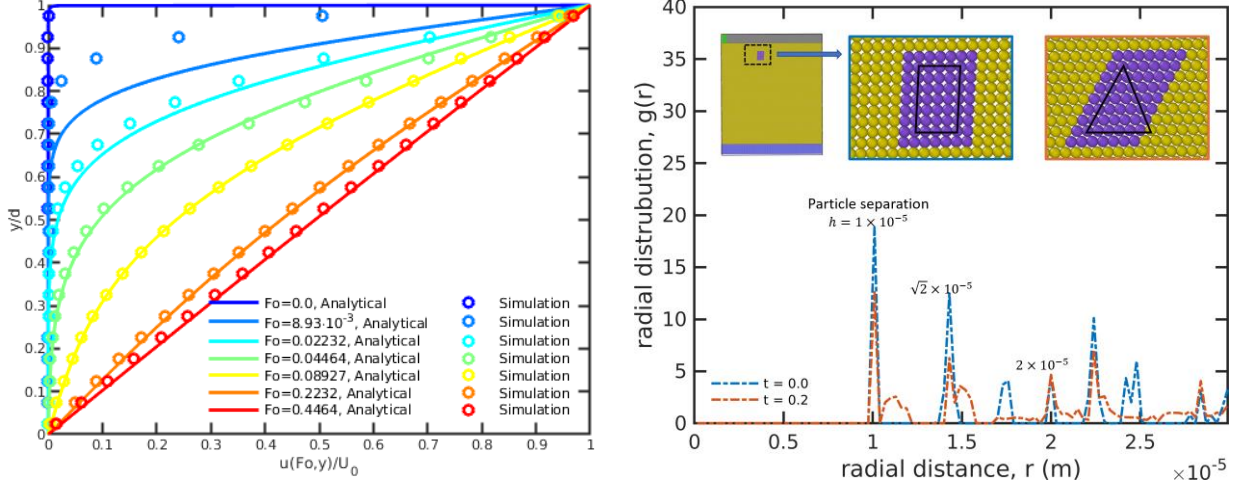


Figure 12. (left) Comparison of simulated profiles with theoretical ones inferred from Eq. 3, for  $t=0.0, 0.0002, 0.0005, 0.001, 0.002, 0.005, 0.01 \text{ s}$  and  $v=0.001 \text{ m/s}$  (see text for details). (right) Radial distribution functions of SPH particles at  $t=0$  and  $0.2 \text{ s}$ . The inset shows the tracking of SPH particles at the same times.

The shape of all simulated profiles matched the analytical ones given by Eq. 3, but without referring to a single  $v$  value. For  $Fo$  values close to  $Fo_{1/2}$  and onwards, the errors were within numerical errors (1-2%). On shorter periods, the profiles were delayed; the layers above the central line were not theoretically translating as fast as expected. Further insights are plotted in the right part of Figure 12 by tracking the SPH particles in the vicinity of the top layer and by following the evolution of their radial distribution. The results suggest that a packing transition was propagating from top to bottom. Layers adopted a hexagonal packing progressively at the beginning of the simulation. It is, however, necessary noticing that it is not a dense packing as the SPH particles displaced occur only horizontally (no particle intercalation). Streamlines remained almost horizontal far from walls, so two adjacent layers recovered a square lattice periodically at a steady state. When shear was applied, the radial distributions show that arrangement tended to be looser with a broadening of the distances to the first and second neighbors. The necessary extra free volume to reorganize particles was brought firstly by the kernel (overlapping are accepted) and secondly by rearranging SPH particles in contact with rigid ones. They adopt during the transition

a hexagonal packing (they move a little up and right) with precisely two Hertz contacts (result not shown but illustrated in Figure 10). The observed lag-time corresponded to the required time to shift top SPH particles from half their radius.

Based on a single simulation, it is difficult to conclude on the full Newtonian character or Stokes character of the SPH fluids. Indeed, second-order tensors are not calculated (we used a Lagrangian method updated at each time step) so that the linearity between the viscous stresses and the local strain rates. From a causal point of view and immediately after the transition period to get good contact with the walls, the reference simulation reproduces an essential feature for Stokes flows and some linear theories, its reversibility in time: opposite causes have opposite effects. Moving the top layer in the opposite direction replaced the particles in their previous positions, such as time was reversed. This feature is stable while no vacancy is introduced in the flow. If not, the diffusion of the vacancy would have made it irreversible.

### *Mechanistic interpretation*

Kinematic viscosity,  $\nu$ , scales time in response to a perturbation, which does not convert the fluid potential or elastic energy into kinetic energy (first principle of thermodynamics), but instead on how the kinetic energy is dissipated (second principle of thermodynamics). What is commonly referred to as viscous force or stress is an effective force or stress that justifies the retarded flow with respect to the disturbance. The concept of retard is independent of the underlying physics. In our Couette simulation, the collisions are not frontal, and the viscous flow results from the “tangential” component of the net force resulting from the interactions with the neighboring particles. The viscosity derived from one simulation becomes an intrinsic property of the SPH fluid if it verifies some invariance with the channel geometry, *e.g.*,  $d$ , and the velocity of the top rigid particles,  $U_0$ . It is associated with a Newtonian behavior if the value of  $\nu$  does not depend on  $U_0/d$ . Due to the partial compressibility of SPH fluids, other invariances are also expected, such as  $\frac{\hat{\nu}}{q_1} \Big|_{h, c_0, q_2=0} = C^{te}$ ,  $\frac{\hat{\nu}}{c_0} \Big|_{h, q_1, q_2=0} = C^{te}$ ,  $\frac{\hat{\nu}}{h} \Big|_{c_0, q_1, q_2=0} = C^{te}$ . These invariances are justified in §3.1 and Eq. 2, where  $\hat{\nu}$  is the estimated viscosity and not the theoretical fluid one. In particular, the size of the particle ( $h$ ) and the speed of the sound ( $c_0$ ) controls at which rate the SPH fluid can rearrange to fit the shape of the moving wall.  $q_1$  acts only between neighboring SPH particles and only when the SPH particles are coming closer to each other. In other words, the critical question is: are we capable of separating and relating the time scale associated with the rigid wall, which causes the flow from the time scale associated with the SPH fluid and determines the correct viscosity effects?

For viscous fluids (water, oil) and at the small scales considered (a few tens of micrometers to one millimeter), we are discussing retard effects at the scale of a few particles. There are two pitfalls to avoid.

- First of all, our simulations are 2D and not 3D, the number of neighbors is smaller (fewer interactions), and the transverse rarefaction waves oscillate only along one direction (only  $y$  since along  $z$  a periodic boundary condition is applied). Therefore, one can expect lower viscosities when considering only a 2D fluid instead of a real-life 3D fluid. The same behavior applies to contacts with rigid wall particles.
- Secondly, the steady-state quality deserves as much attention as the estimated kinematic viscosity value. A slip condition can affect the macroscopic velocity gradient.

### 5.3 Parameters effecting of the kinematic viscosity

The control variables method (one single parameter is changed at a time) was used to evaluate the effects of  $(U_0, d, q_1, c_0, h)$ . For each quantity  $x$ , six levels were studied so that:  $\frac{x}{\bar{x}} = 0.1, 0.2, 0.5, 2, 5, 10$  where  $\bar{x}$  is the reference value. In total, 31 conditions ( $5 \times 6 + \text{reference}$ ) were explored. The results of 20 sets are plotted in Figure 13 on a semi-log-scale but compared with a linear model. The effects of  $h$  are not shown as additional coarsening transformed the walls into rough surfaces with properties not captured by the simple laminar flow solution (see Eq. 3). Corresponding Reynolds,  $Re = \frac{U_0 d}{\nu}$ , and Mach,  $\frac{U_0}{c_0}$ , numbers are reported to facilitate the understanding. The reader should be aware that tested conditions cover extreme conditions for SPH fluids: no inertial flow ( $Re < 0.22$ ), strong discrepancy between the flow and sound speeds ( $Ma < 0.05$ ). The estimated kinematic viscosity is only based on  $t_{1/2}$  and does account for any lag correction.

#### *Mechanistic interpretation*

The effects of  $U_0$  and  $d$  were not similar and therefore could not be attributed to inertial forces ( $U_0 d$ ). For velocities greater than reference and gaps smaller than reference,  $\hat{\nu}$  was underestimated, and the SPH flow reacted more slowly than its ideal counterpart. The deviation is to be traced back to the interactions with the wall. Too high velocities do not allow the density to fluctuate sufficiently when the speed of sound is too high. The SPH particles near the wall do not have time to explore how to lodge themselves between the rigid particles. This effect will be analyzed later by examining how information propagates between particles. The effect of distance is similar; the density fluctuations occur vertically in the gap. One could say that as for  $h$ , one must keep enough



resolution to describe the flow in a macroscopic sense. The parameters  $q_1$  and  $c_0$  behave like the theory and can be used as two linear correctors to obtain the desired viscosity in the laminar regime even at very low Reynolds number.

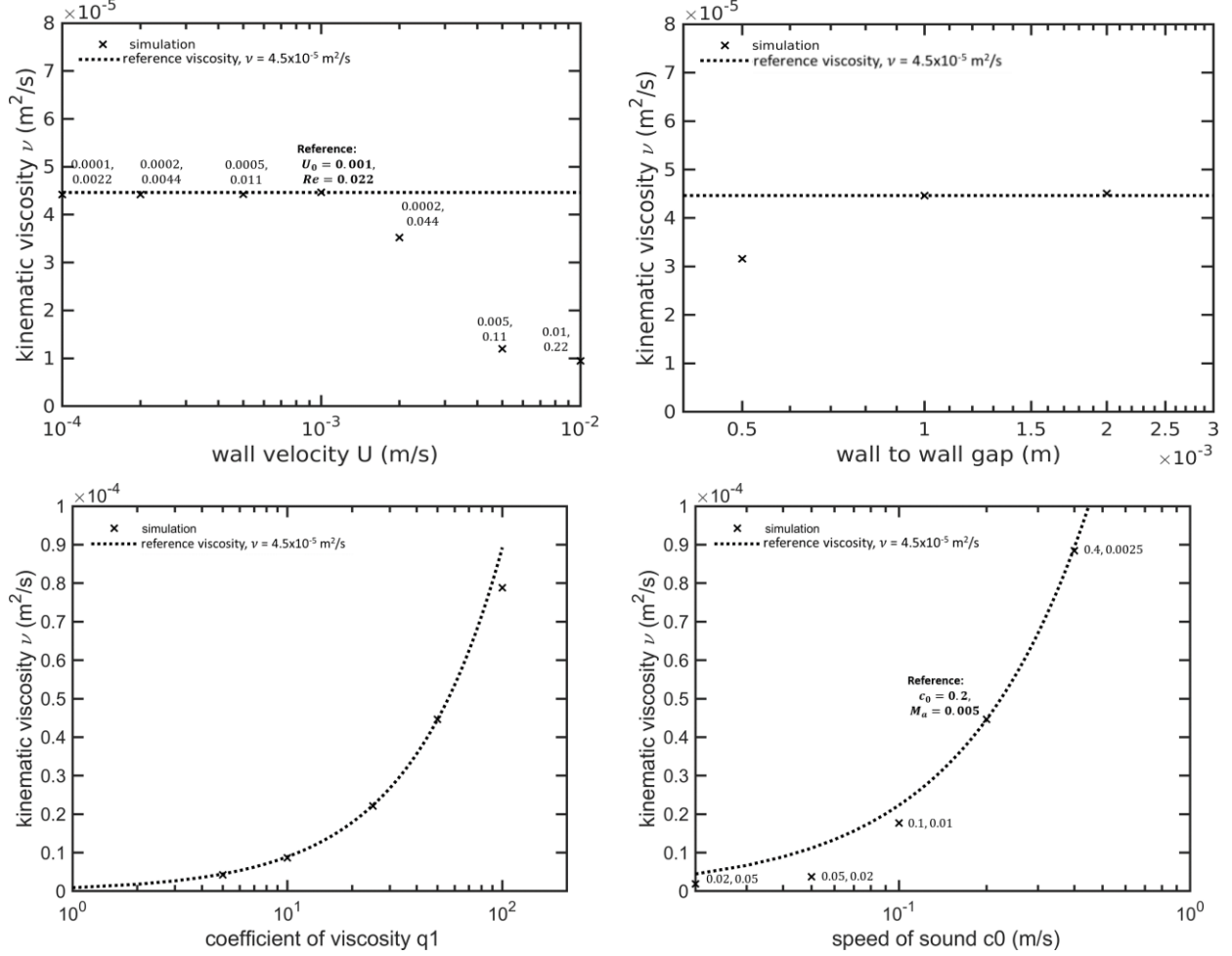


Figure 13. Effects of the main studied parameters ( $U_0, d, q_1, c_0$ ) on the estimated kinematic viscosity (see text for details).

## 5.4 Optimization directions

### 5.4.1 Problem statement

Contrarily to intuition, the SPH fluid remains compressible, particularly close to walls. This effect is shown for the reference simulation in Figure 14. Six SPH layers are required to reach a proper convergence towards the bulk density. This optimal packing is reached after the initial equilibration and is maintained when the flow is started. The transitional regions in contact with moving and non-moving evolve subsequently symmetrically. A drop of density is observed with time and is associated with the periodic boundary conditions. Before the flow starts, a square packing is

enforced at the boundaries (no particle is overlapping); it will be progressively lost with the developed flow showing a drop of density. It is reduced if the length of the channel is increased. For best results, the channel length should be ten times longer than the gap.

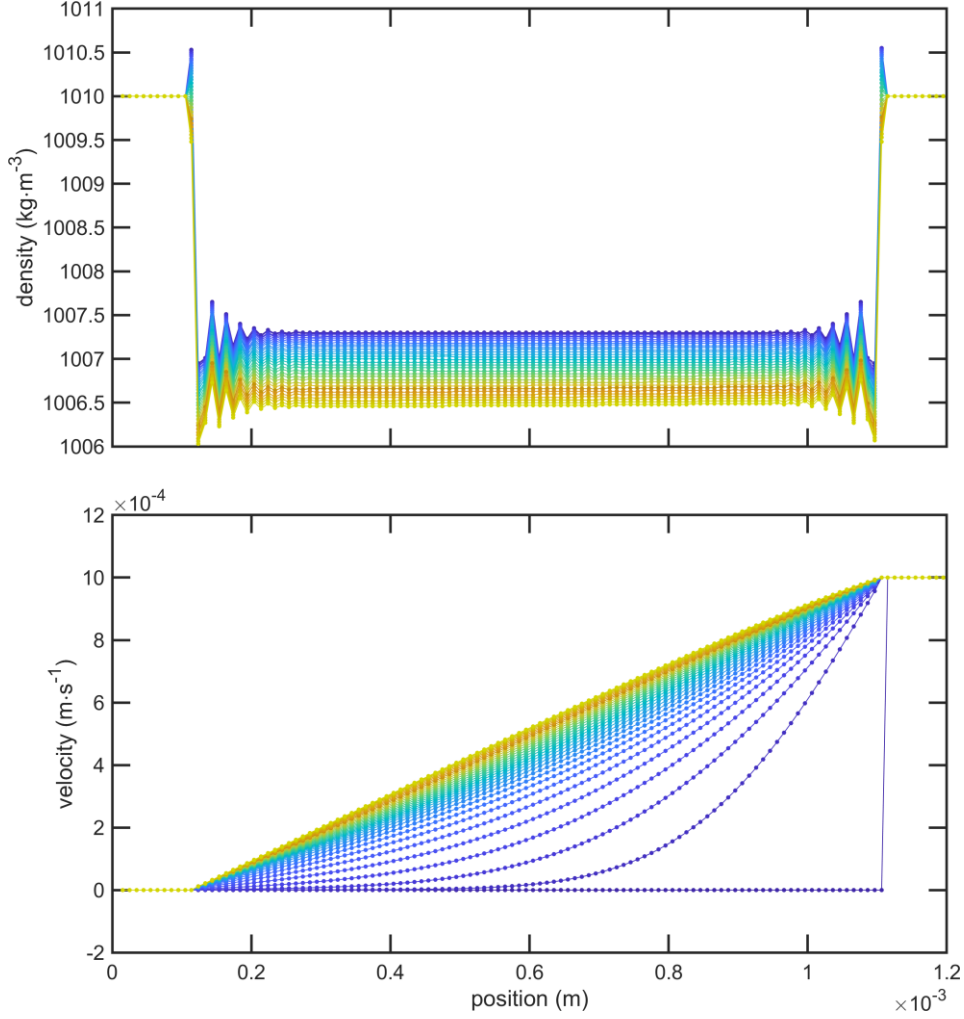


Figure 14. Ensemble-averaged density and horizontal velocity as a function of the vertical position for the reference simulation. The same duration separates all profiles.

#### 5.4.2 Suggested strategies for better control of viscosity

Two directions of optimization are necessary for the studied conditions and according to the results already presented:

- The time for the SPH particles to conform to the surface shape can be directly evaluated by looking at how the local slip ( $U_0 - u(y = d, t)$ ) between the contacting SPH layer and the rigid layer reduces. An analytical correction can be performed *a posteriori* if necessary.
- Physically, the speed of sound can be adjusted to allow the propagation of transverse waves that will allow the adjustment of the two layers during the relaxation time.

The concept of a sliding effect fading with time is exemplified in Figure 14. A second-order relaxation is shown with significant damping. Damping times were consistent with deviations observed on the kinematic viscosity: more slip and lower kinematic viscosity. Strong damping confirmed the crucial role of the local packing in the vicinity of the walls. This reordering is faster than the propagation of momentum between the two walls. If the speed of the sound is enough and the size of particles is small compared to the gap length ( $d \gg h$ ), the lag time (proportional to  $\frac{h}{c_0}$ ) can be made negligible compared to the momentum diffusion time  $\frac{d^2}{\nu}$ . That is to say that  $h$  should fulfill:

$$h \ll \frac{c_0 d^2}{\nu} = \frac{Re}{Ma_{recommended}} d \quad Eq. 8$$

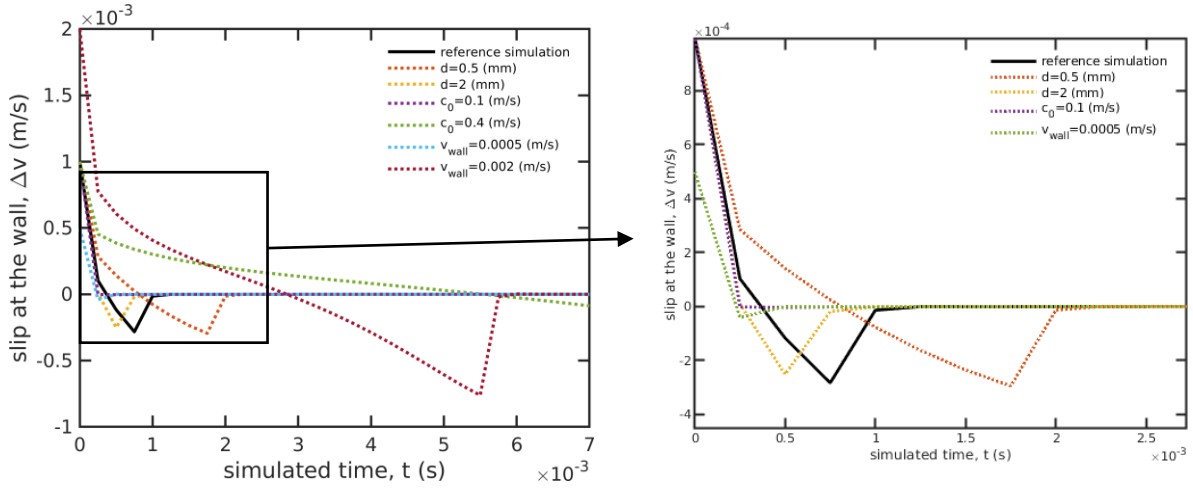


Figure 15. (left) Curve of the relative velocity of the particles immediately adjacent to the moving plate as a function of simulation time and (right) magnified view of selected area in box.

By choosing a recommended Mach number,  $Ma_{recommended}$ , of 0.1, the condition  $d \gg h$  leads to an optimal viscosimeter for kinematic viscosity estimation when it verifies  $Re \ll 0.1$ . This condition guarantees the absence of corrections a posteriori. An illustration of the achievable improvements is shown in Figure 15. The results match the theory well and can be used to parameterize an SPH fluid. However, the previous problems will occur again in complex simulations when the characteristic dimensions are not perfectly known. The biases remain quantifiable as well as the possible gain. Lowering  $h$  will always be beneficial, and comparing two results with different  $h$  values will enable rapid estimation of the cost-to-accuracy ratio.

Velocity gradients are well reproduced with no significant slip in contact with the moving rigid particles (top) or immobilized ones (bottom). The gradients are, however, not correctly defined in these layers at a scale lower than the particle diameter. There are two reasons for explaining an  $C_0$

approximation (with discontinuous derivatives) of the velocity field instead of  $C_1$  (with continuous derivatives). Though it may be seen as a poor performance compared to the Eulerian approach, it was precisely the sought effect. In the flow direction, the hertz contacts associated with the hexagonal packing are sufficiently rigid to counterbalance any fluid force, which would provoke a translation back or forth of SPH particles. No-slip condition is therefore enforced naturally as soon as a dense packing is achieved. In the direction perpendicular to the flow, the shear rate is underestimated due to the absence of SPH particles attached to the moving wall. For smooth surfaces, these effects are acceptable if the particle size ( $h$ ) is chosen small compared to the characteristic length of the flow or the thickness of the boundary layer.

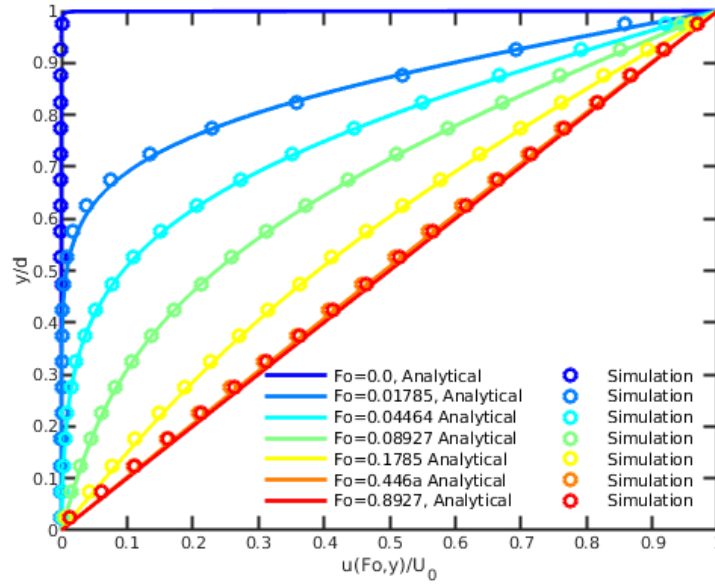


Figure 16. Comparison of SPH simulations transient velocity profile to that of the analytical solution for of a Newtonian fluid being sheared with  $c_0 = 0.4$  m/s.

## 6 Conclusions

The presented work focused on evaluating the characteristic time scale for the propagation of viscous perturbations in the laminar regime ( $Re < 1$ ) is part of a much larger scheme of construction of a generic tool for the simulation of the deconstruction of food. It has led to many discussions on the origin of causes and the reality of observed behaviors. First, coarse-grained simulation is not a mathematical solution technique. It does not have to provide an exact value to a set of initial and boundary conditions. It is a resolution of the transfer equations using physical simulations and details of intermediate description between the molecules and the macroscopic scale. In this work, only methods, so-called Molecular Dynamics like, were used; they implement exclusively radial forces (centrifugal or centripetal). Secondly, it is necessary to realize that no collective property (resulting from interactions) exists *a priori* beyond the scale of a particle or the interaction between two particles. Collective properties such as transport properties (diffusivity, viscosity) emerge from interactions during the simulation: collisions and packing. Although we have relied extensively on smoothed particle hydrodynamics methods, with certain analogies with continuum mechanics and techniques of mathematical resolution of partial differential equations by collocation methods, we have also introduced Hertz contacts which break the fuzzy description of simulated fields (pressure, density) and force a particle behavior. This combination has been more particularly explored. In the context of oral processing, it would allow representing all or part of the mouth (palate, teeth, tongue) with meshed surfaces covered with rigid particles animated by a displacement and possibly by deformations (using a total Lagrangian description).

The interaction between rigid particles and SPH particles has been studied for 2D transient planar Couette flows and from an initial trivial configuration where all particles have the same size and are arranged in a square packing. This configuration was chosen because it would allow the direct use of microscopic images to map the particles. The objectives were multiple:

- to ensure that the flow causality was well reproduced with a sound reproduction of the velocity gradient.
- to ensure the existence of an apparent viscosity relatively independent of the operating conditions (velocity, gap length)
- to set up a numerical viscometer that can be used to validate a fluid before production or to tabulate the relations between kinematic viscosity and the simulation parameters in advance.

Provided that the system is pre-equilibrated and the speed of sound is correctly parameterized to the speed of momentum propagation, causality and viscous time scales can be reconstructed. These objectives are fulfilled, primarily since the conclusions of this work are already implemented in a

*generic()* class for Pizza3. The studied conditions offer a viscosity parameterization for food components such as edible oil ( $5 \times 10^{-5} \text{ m}^2/\text{s}$ ) with large particles. For water and low viscosity fluids, smaller particles should be preferred instead.

This work, which still needs to be confirmed by a series of 3D simulations (i.e., with particles along  $z$ ), shows the interest in mixing particles to create or tune interactions. This effect, called salting, is already used in the Martini force field to avoid the crystallization of water with an essentially attractive force field (centripetal). Similar effects can be sought to create non-Newtonian behaviors. Rigid particles can block or propagate the momentum depending on whether they are suspended in the flow or constitute walls. The use by the team of 3D meshes to reproduce arbitrary surfaces which are back mapped onto rigid particles is a good follow-up. This work's results will apply if the triangles are equilateral and allow a hexagonal packing.

The internship continues with studying the mutual diffusion between bile salts and vitamins dispersed in fat globules. The simulations were performed by the team with the Martini force field. They must be extended with Dissipative Particle Dynamics methods. A link with this work will be made by testing the behavior of a DPD fluid in the viscometer.

## References

- [1]. Datta, A. K., van der Sman, R., Gulati, T., & Warning, A. Soft matter approaches assemblers for food macroscale simulation. *Faraday Discussions*, (2012).
- [2]. Thompson, A. P. et al. LAMMPS - a flexible simulation tool for particle-based materials modeling at the atomic, meso, and continuum scales. *Comput. Phys. Commun.* 271, (2022).
- [3]. Diaz, A. et al. A parallel algorithm for the concurrent atomistic-continuum methodology. *J. Comput. Phys.* 463, 111140 (2022).
- [4]. Ho, Q.T.; Carmeliet, J.; Datta, A.K.; Defraeye, T.; Delele, M.A.; Herremans, E.; Opara, L.; Ramon, H.; Tijssens, E.; van der Sman, R.; et al. Multiscale modelling in food engineering. *J. Food Eng.* 114, (2013).
- [5]. Bagchi, P. Mesoscale Simulation of Blood Flow in Small Vessels. *Biophys. J.* **92**, 1858–1877 (2007).
- [6]. Lopez, C. A., Uusitalo, J. J., Jong, D. H. De, Gopal, S. M. & Periole, X. The power of coarse graining in biomolecular simulations. **4**, 225–248 (2014).
- [7]. Voth, Gregory A. Coarse-graining of condensed phase and biomolecular systems. CRC press, (2008).
- [8]. Praprotnik, Matej, Luigi Delle Site, and Kurt Kremer. Multiscale simulation of soft matter: From scale bridging to adaptive resolution. *Annu. Rev. Phys. Chem.* 59, (2008).
- [9]. M. P. Allen and D. J. Tildesley, *Computer Simulation of Liquids* (Second Edition), Journal of Molecular Liquids, (2017), p398
- [10]. Alessandri, R., Grünewald, F. & Marrink, S. J. The Martini Model in Materials Science. *Adv. Mater.* **33**, (2021).
- [11]. Guan D, Feng S, Zhang L, et al. Mesoscale simulation for heavy petroleum system using structural unit and dissipative particle dynamics (SU-DPD) frameworks. *Energy & Fuels*, 33(2), (2019).
- [12]. Chen, Y., Zimmerman, J., Krivtsov, A. & McDowell, D. L. Assessment of atomistic coarse-graining methods. *Int. J. Eng. Sci.* **49**, 1337–1349 (2011).
- [13]. Irving, J. H., and John G. Kirkwood. The statistical mechanical theory of transport processes. IV. The equations of hydrodynamics. *The Journal of chemical physics* 18.6, (1950).
- [14]. Kirkwood, John G., and Frank P. Buff. The statistical mechanical theory of solutions. I. *The Journal of chemical physics* 19.6, (1951).
- [15]. Holian, B. L. A History of constitutive modeling via molecular dynamics: Shock waves in fluids and gases. *EPJ Web Conf.* **10**, (2011).

- [16]. James Campbell, Rade Vignjevic, Artificial Viscosity Methods for Modelling Shock Wave Propagation, Predictive Modeling of Dynamic Processes, (2009), pp 349–365.
- [17]. Monaghan, J. J. Simulating Free Surface. *Journal of Computational Physics* vol. 110 399–406 (1994).
- [18]. [GitHub - ovitrac/Pizza3: Fork of Pizza.py toolkit for Python 3.x \(loosely integrated collection of tools for LAMMPS\)](#)
- [19]. Albano, A. et al. How to modify lammmps: From the prospective of a particle method researcher. *ChemEngineering* 5, 1–57 (2021).
- [20]. Li, C., Fu, X., Zhong, W. & Liu, J. Dissipative Particle Dynamics Simulations of a Protein-Directed Self-Assembly of Nanoparticles. *ACS Omega* **4**, 10216–10224 (2019).
- [21]. Gingold, R.A., Monaghan, J.J.: Smoothed particle hydrodynamics: theory and application to non-spherical stars. *Monthly Notices of the Royal Astronomical Society* 181(3), 375–389 (1977).
- [22]. Lucy, L.B.: A numerical approach to the testing of the fission hypothesis. *The Astronomical Journal* 82, 1013 (1977).
- [23]. Monaghan, J.J., Gingold, R.A.: Shock simulation by the particle method SPH. *Journal of Computational Physics* 52(2), 374–389 (1983).
- [24]. Monaghan, J.J.: Simulating free surface flows with SPH. *Journal of Computational Physics* 110(2), 399–406 (1994).
- [25]. Morris, J.P., Fox, P.J., Zhu, Y.: Modeling low reynolds number incompressible flows using SPH. *Journal of Computational Physics* 136(1), 214–226 (1997).
- [26]. Vacondio, R., Altomare, C., Leffe, M.D., Hu, X., Touz'e, D.L., Lind, S., Marongiu, J.-C., Marrone, S., Rogers, B.D., Souto-Iglesias, A.: Grand challenges for smoothed particle hydrodynamics numerical schemes. *Computational Particle Mechanics* 8(3), 575–588 (2020).
- [27]. Violeau, D., Rogers, B.D.: Smoothed particle hydrodynamics (SPH) for free-surface flows: past, present and future. *Journal of Hydraulic Research* 54(1), 1–26 (2016).
- [28]. Lavergne, M.D.D., Young, A.K., Engmann, J., Hartmann, C.: Food oral processing—an industry perspective. *Frontiers in Nutrition* 8 (2021).
- [29]. Alessandri, R. *et al.* Pitfalls of the Martini Model. *J. Chem. Theory Comput.* **15**, 5448–5460 (2019).
- [30]. Praprotnik, M., Matysiak, S., Site, L. D., Kremer, K. & Clementi, C. Adaptive resolution simulation of liquid water. *J. Phys. Condens. Matter* 21, 499801–499801 (2008).



- [31]. Zavadlav, J., Marrink, S. J. & Praprotnik, M. Adaptive Resolution Simulation of Supramolecular Water: The Concurrent Making, Breaking, and Remaking of Water Bundles. *J. Chem. Theory Comput.* **12**, 4138–4145 (2016).
- [32]. Alberto Dutra Fraga Filho, C. Smoothed Particle Hydrodynamics Fundamentals and Basic Applications in Continuum Mechanics.(2018).
- [33]. Wang, J. S., Zhang, X. D. & Fang, F. Z. Numerical study via total Lagrangian smoothed particle hydrodynamics on chip formation in micro cutting. *Adv. Manuf.* **8**, 144–159 (2020).
- [34]. Marrink, S. J. & Tieleman, D. P. Perspective on the martini model. *Chem. Soc. Rev.* **42**, 6801–6822 (2013).
- [35]. Liu, M. B., Liu, G. R., Zhou, L. W. & Chang, J. Z. Dissipative Particle Dynamics (DPD): An Overview and Recent Developments. *Arch. Comput. Methods Eng.* **22**, 529–556 (2015).
- [36]. Ye, T., Pan, D., Huang, C. & Liu, M. Smoothed particle hydrodynamics (SPH) for complex fluid flows: Recent developments in methodology and applications. *Phys. Fluids* **31**, (2019).
- [37]. Fulk, David Allen, P. D. A numerical analysis of smoothed particle hydrodynamics. *Air Force Inst. Technol.* 274 (1994).
- [38]. VonNeumann, J. & Richtmyer, R. D. A method for the numerical calculation of hydrodynamic shocks. *J. Appl. Phys.* **21**, 232–237 (1950).